Journal of Applied Polymer Science

Nonisothermal Crystallization Behaviors of Biodegradable Double Crystalline Poly(butylene succinate)-Poly(ethylene glycol) Multiblock Copolymers

Cai-Li Huang, Jian-Bing Zeng, Ling Jiao, Ke-Ke Yang

Center for Degradable and Flame-Retardant Polymeric Materials (ERCPM-MoE), College of Chemistry, State Key Laboratory of Polymer Materials Engineering, National Engineering Laboratory of Eco-Friendly Polymeric Materials (Sichuan), Sichuan University, Chengdu 610064, China

Correspondence to: K.-K. Yang (E-mail: kkyangscu@126.com)

ABSTRACT: Nonisothermal crystallization behaviors of both poly(butylene succinate) (PBS) and poly(ethylene glycol) (PEG) segments within PBS-PEG (PBSEG) multiblock copolymers were investigated by differential scanning calorimetry (DSC). The nonisothermal crystallization kinetics of both PBS and PEG segments were analyzed by Avrami, Ozawa, and Mo methods. The results showed that both of Avrami and Mo methods were successful to describe the nonisothermal crystallization kinetics of PBS and PEG segments. The results of crystallization kinetics indicated that the crystallization rate of PBS segment decreased with PBS segment content and/or L_{PBS}, while that of PEG segment decreased with $M_{n,PEG}$ or F_{PEG}. © 2014 Wiley Periodicals, Inc. J. Appl. Polym. Sci. **2014**, *131*, 40940.

KEYWORDS: biodegradable; copolymers; crystallization; kinetics

Received 20 January 2014; accepted 27 April 2014
DOI: 10.1002/app.40940

INTRODUCTION

Bio-based and biodegradable polymers have received growing attention from both industry and academia during the past decades because of the increasing concerns of sustainable environment.[1–5] Among them, aliphatic polyesters and poly(ether-ester)s are of high importance as they show widely potential applications in both biomedical materials and are general environmentally friendly.[6,7] Of all the biodegradable thermoplastics, poly(butylene succinate (PBS) is regarded as one of the most promising materials for its high mechanical strength, complete biodegradability, and renewability.[8–10] In addition, as a commercially available aliphatic polyester, it has good thermal stability.[11] Poly(ethylene glycol (PEG) is nontoxic and can be used in human body. In the past decades, PEG-based polyester-polyether type block copolymers, which could be used in medical applications such as implantation and wound treatment, and as controlled-release drug carriers, have been widely studied.[12–16]

Based on the above discussions, the biodegradable aliphatic copolyesters which contain PBS and PEG segments were synthesized by direct polycondensation, and the crystallization and biodegradable behaviors were studied.[17,18] More importantly, shape memory PBS-PEG (PBSEG) multiblock copolymers have been prepared.[19] The permanent netpoints consisted of the physical crosslinks of PBS crystals because of PBS segment's high tendency to crystallize, while PEG segment was used as soft segment and its melting point determined the transition temperature. The PEG segment endowed PBSEG multiblock copolymers high ductility and improved hydrophilic property. Besides, mutual effect of PBS and PEG segments on the crystallization behavior and morphology was discussed through crystallization kinetics and morphology investigation.[20] What is more, fractional crystallization behavior and nucleation mechanism of PEG segment within PBSEG with different compositions were systematically studied.[21]

As for those biodegradable semicrystalline polyesters and poly(-ether-ester)s applied in practical field, the degradation rate and mechanical properties are critical. Crystallization kinetics plays an important role in these properties of semicrystalline polymers. For example, it has been found that the melt-quenched PBS showed slower hydrolytic degradation rate than the isothermally crystallized PBS although they had similar degree of crystallinity.[22] The difference of biodegradation rate in the two samples was attributed to the different crystallization kinetics. And we can obtain brittle/flexible material with high/low crystalline degree through tuning the crystallization kinetics. Therefore, it is important to study the crystallization kinetics in

Additional Supporting Information may be found in the online version of this article.

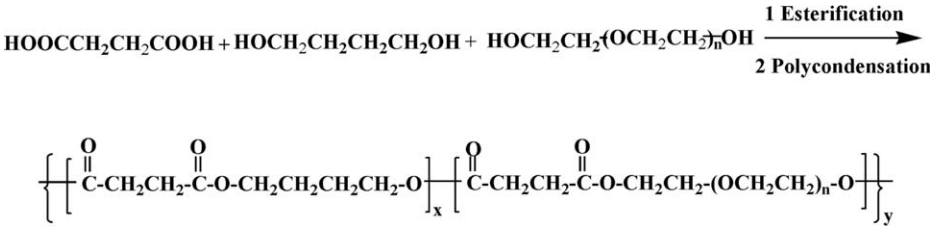

Scheme 1. The preparationroute of PBSEGsand its chemical structure.

biodegradable semicrystalline polymers. It is well-known that the crystallization kinetics is separated into isothermal and nonisothermal crystallization. Indeed, the nonisothermal crystallization kinetics is very important toward the processing of polymers because the industrial processing is always nonisothermal, such as extrusion, injection molding and blow molding.[23–35] Although crystallization behaviors of biodegradable polymer blends and di- or tri- block copolymers have been extensively investigated before,[36–46] less attention has been paid to the crystallization behaviors of biodegradable double crystalline multiblock copolymers that contain different chain segment length. The crystallization behaviors of double crystalline multiblock copolymers, where the crystallization of one component may affect the second component, are even more complicated than blends and di/tri- block copolymers. Furthermore, the investigation of nonisothermal crystallization kinetics on biodegradable double crystalline multiblock copolymers is seldom studied.

The present work focuses on nonisothermal crystallization behavior of double crystalline PBSEG multiblock copolymers. The nonisothermal crystallization kinetics of PBSEGs was characterized by DSC and analyzed by the Avrami method and Mo method. The aim of this article is to provide some fundamental data for a thorough understanding of the nonisothermal crystallization behavior of double crystalline multiblock copolymers.

EXPERIMENTAL

Synthesis

PBSEG multiblock copolymers were synthesized by a two step transesterification reaction, and the preparation route is shown in Scheme 1. These procedures were reported previously.[19] First, calculated amounts of 1,4-butanediol, succinic acid, and PEG (1 : 1.05 by mole ratio of diacid to diol) were added into a 250 mL three-necked round-bottomed flask equipped with water separator, mechanical stirrer, and nitrogen inlet pipe. The monomer mixture was melted and stirred for 4 h at 190°C to complete the esterification reaction. Then, after a suitable amount of catalyst $Ti(OC_4H_9)_4$ was introduced into the flask under dry nitrogen, the polycondensation was carried out at 230°C with vacuum of 40 Pa for 4–7 h. The products were purified by dissolving in chloroform and then precipitating in excessive ether. The white powder products were dried under vacuum. Table I lists the molecular weight characterization data obtained by gel permeation chromatography (GPC) and ^{1}H-NMR.

Nonisothermal Crystallization

The nonisothermal crystallization behaviors of PBSEGs were investigated by DSC using a TA DSC-Q200 instrument. The samples were first heated to 140°C, kept at that temperature for 3 min in order to erase thermal history, and then cooled to −20°C at various cooling rates ranging from 2.5°C/min to 20°C/min. The exothermal curves of heat flow as a function of temperature were recorded and analyzed.

RESULTS AND DISCUSSION

In order to learn the influence of PEG segment fraction and segment chain length on nonisothermal crystallization behavior of PBSEG, five samples ($PBSEG_{2K\text{-}60}$, $PBSEG_{6K\text{-}61}$, $PBSEG_{10K\text{-}58}$, $PBSEG_{10K\text{-}50}$, and $PBSEG_{10K\text{-}38}$) are selected. Among them, $PBSEG_{2K\text{-}60}$, $PBSEG_{6K\text{-}61}$, and $PBSEG_{10\text{–}58}$ with almost same PEG content have different segment chain lengths, whereas the other two samples, i.e. $PBSEG_{10K\text{-}50}$ and $PBSEG_{10K\text{-}38}$, have same segment chain length with $PBSEG_{10\text{–}58}$ but different PEG contents. Here, we obtained the segment chain length of PBS segment from the following equation, and the values are listed in Table I:

Table I. Designation, Composition, and Molecular Weight of PBSEGs

Sample name	$M_{n,PEG}$ (10^3 g/mol)	f_{PEG}[a] (wt %)	F_{PEG}[b] (wt %)	$M_{n,PBSEG}$[c] (10^4 g/mol)	PDI[c]	L_{PBS}
$PBSEG_{2k\text{-}60}$	2	50	60.50	7.36	3.27	7
$PBSEG_{6k\text{-}61}$	6	50	61.42	8.61	3.31	21
$PBSEG_{10k\text{-}58}$	10	50	58.31	7.28	3.85	41
$PBSEG_{10k\text{-}50}$	10	40	50.43	5.02	3.61	57
$PBSEG_{10k\text{-}38}$	10	30	38.00	9.52	3.21	94

[a] f_{PEG} presents feed ratio of PEG-diol.
[b] The weight fraction of PEG segment which was calculated by ^{1}H-NMR spectra.
[c] $M_{n,PBSEG}$ and PDI were determined by GPC with PS standards in chloroform.

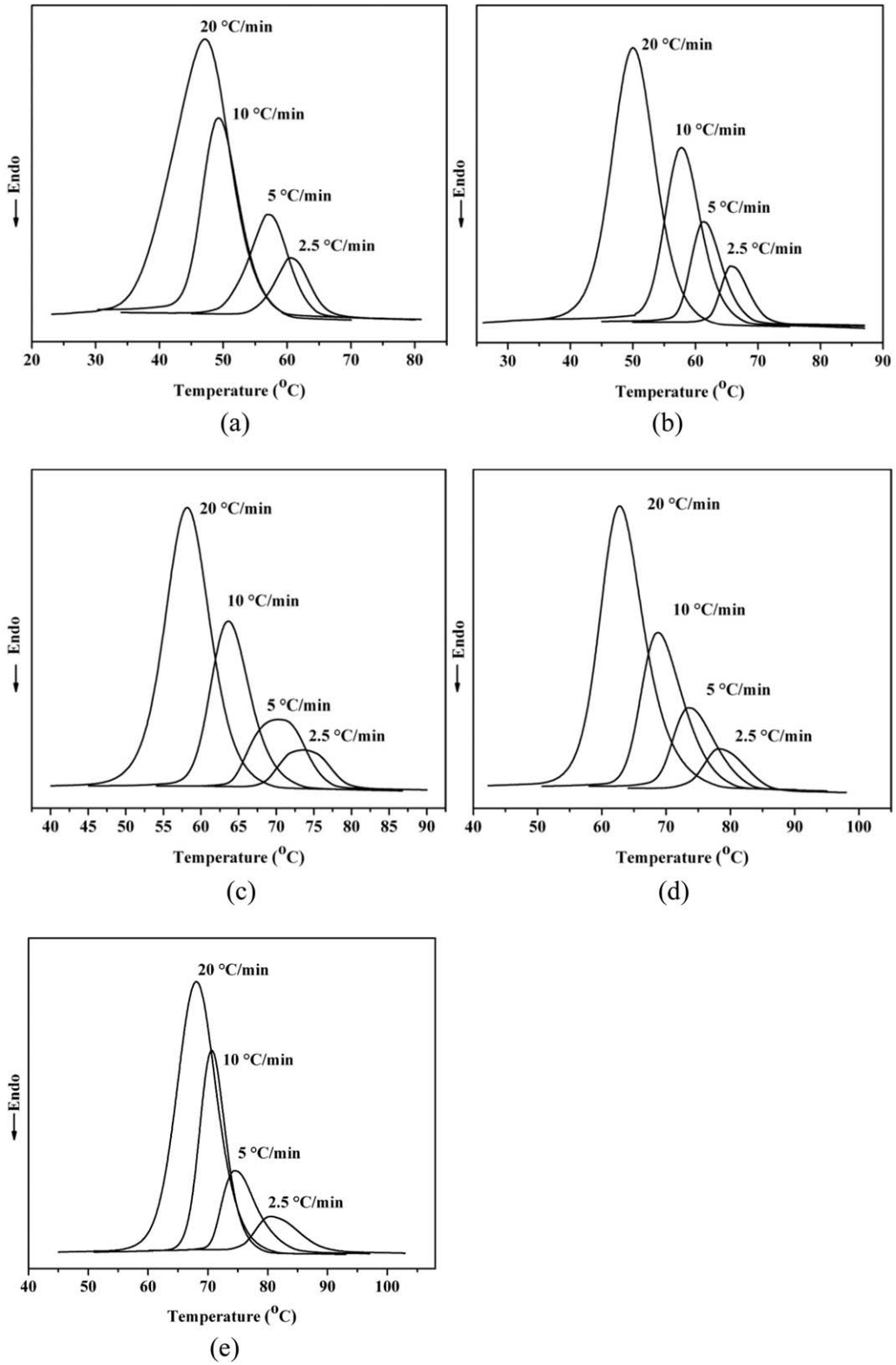

Figure 1. Nonisothermal crystallization curves of PBS segment within (a) $PBSEG_{2K\text{-}60}$, (b) $PBSEG_{6K\text{-}61}$, (c) $PBSEG_{10K\text{-}58}$, (d) $PBSEG_{10K\text{-}50}$, and (e) $PBSEG_{10K\text{-}38}$ at different cooling rates.

$$L_{PBS}=\frac{M_{n,PEG}}{172}\left(\frac{1}{F_{PEG}}-1\right)-\frac{84}{172} \quad (1)$$

From previous studies,[20] both PBS and PEG segments of these five samples showed large crystallization exothermic peaks when cooling from melt. Here, the analysis of nonisothermal

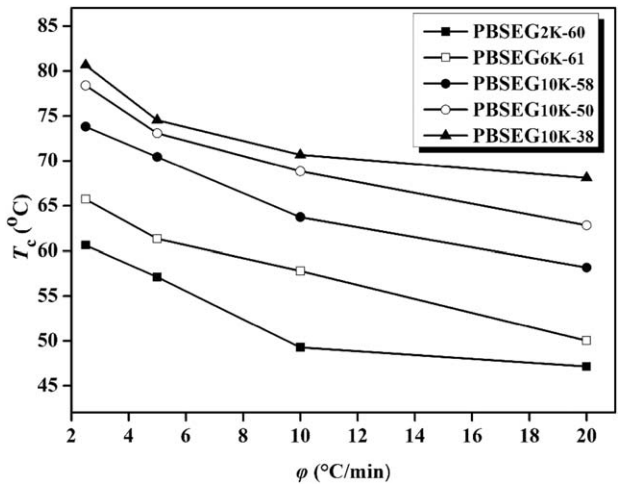

Figure 2. The crystallization peaktemperature of PBS segmentwithinPBSEG at various cooling rates.

crystallization kinetics of PBS and PEG segments within PBSEG is divided into two parts.

Nonisothermal Crystallization Kinetics Study of PBS Segment Within PBSEG

The investigation of the nonisothermal crystallization behavior of semi-crystalline polymers is of high technical importance as most practical processes such as injection, extrusion, and other molding is performed under nonisothermal conditions.[47] In the present study, the nonisothermal crystallization kinetics of PBS segment within PBSEG is investigated firstly. Figure 1 shows the DSC cooling curves of PBSEGs which were cooled from melt state at various rates (ϕ). Typical exothermic peaks were observed, and they shifted to lower temperatures and became wider as increasing the cooling rate for all samples. The crystallization peak temperatures (T_c) are summarized in Figure 2. The values of T_c gradually decreased from $PBSEG_{10K-38}$ to $PBSEG_{10K-50}$, $PBSEG_{10K-58}$, $PBSEG_{6K-61}$, and $PBSEG_{2K-60}$ regardless of the cooling rate. When the molecular weight of PEG diol ($M_{n,PEG}$, or the segment chain length of PEG segment) kept at a constant, the content of PBS segment and the average chain length of the PBS segment (L_{PBS}) would decrease with the increase of the content of PEG segment (F_{PEG}).[19] Thus, the values of T_c decreased from $PBSEG_{10K-38}$ to $PBSEG_{10K-50}$ and $PBSEG_{10K-58}$. Besides, the decrease of T_c from $PBSEG_{10K-58}$ to $PBSEG_{6K-61}$ and $PBSEG_{2K-60}$ was attributed to the decrease of L_{PBS}, which was in agreement with previous work.[20]

The relative crystallinity (X_t) of PBS segment within $PBSEG_{2K-60}$, $PBSEG_{6K-61}$, $PBSEG_{10-58}$, $PBSEG_{10K-50}$, and $PBSEG_{10K-38}$ as a function of temperature is shown in Figure 3. X_t was calculated by integration of the exothermic peak during the cooling process according to the following equation:

$$X_t = \frac{\int_{T_0}^{T} \left(\frac{dH_c}{dT}\right) dT}{\int_{T_0}^{T_\infty} \left(\frac{dH_c}{dT}\right) dT} \quad (2)$$

where T_0 and T_∞ refer the temperatures at the onset and end of crystallization, respectively, and dH_c/dT represents the heat flow at temperature T.[48] It can be seen that the typical sigmoidal shape curves for all samples were obtained, suggesting that fast primary crystallization as well as slow secondary crystallization appeared at the early and later stages, respectively, and the curves shifted to lower temperature range with the increase of cooling rate.

Although the well-known Avrami method is often used to study the isothermal crystallization kinetics of crystalline polymers, it can also be directly used to describe the nonisothermal crystallization.[23,29,49,50] The Avrami equation assumes that the relative degree of crystallinity develops with crystallization time as

$$1 - X_t = \exp(-Zt^n) \quad (3)$$

where X_t is the relative crystallinity calculated by eq. (2), n is the Avrami exponent, Z is the crystallization rate constant, and t is crystallization time.[51] Equation (3) can be rewritten as

$$\lg(-\ln(1 - X_t)) = \lg Z - n \lg t \quad (4)$$

Similarly to the description of isothermal crystallization kinetics, the values of Z and n were obtained from a straight line by plotting $\lg(-\ln(1-X_t))$ versus $\lg t$ from $X_t = 0.05$ to 0.80 for different cooling rates, shown in Figure 4. From Figure 4, it can be seen that a series of parallel lines were obtained for various cooling rates, suggesting that Avrami method could describe the nonisothermal crystallization kinetics of PBS segment within PBSEG. The values of the two parameters n and Z were derived from the slopes and intercepts of the fitted straight lines, and the results are summarized in Table II. Here, the exponent n in nonisothermal crystallization kinetics has the different physical meaning compared with isothermal crystallization kinetics because of the different conditions.[29] Despite of that, it could also provide important information in the mechanism of nonisothermal crystallization. The average values of Avrami exponent of $PBSEG_{2K-60}$, $PBSEG_{6K-61}$, $PBSEG_{10-58}$, $PBSEG_{10K-50}$, and $PBSEG_{10K-38}$ were 7.05, 6.48, 5.23, 3.61, and 3.26, respectively. Although one can hardly predict the mechanism of nonisothermal crystallization directly from the Avrami exponent, the higher values in $PBSEG_{2K-60}$ and $PBSEG_{6K-61}$ may still indicate the difference of crystallization mechanism. From $PBSEG_{10K-38}$ to $PBSEG_{10K-50}$, $PBSEG_{10K-58}$, $PBSEG_{6K-61}$, and $PBSEG_{2K-60}$, according to our previous work,[20,21] L_{PBS} of the copolymers reduced in this order. This reduction resulted in the decrease of PBS microdomains and mobility of PBS segment, and the PBS segment distribution became increasingly disordered. Thus, this may be the reason that Avrami exponent of $PBSEG_{2K-60}$ is larger than $PBSEG_{10K-38}$. Besides, the morphology formed by PBS segment within $PBSEG_{2K-60}$ was 2-dimentional aggregations, while that of $PBSEG_{10K-38}$ displayed typical spherulite.[20] This can be also used to explain why the Avrami exponent of $PBSEG_{2K-60}$ is larger. In Table II, as expected, the values of crystallization rate constant (Z) of all samples decreased with the ϕ. A normalized rate constant, $k = Z^{1/n}$, which is independent of the Avrami exponent, was evaluated for comparison.[52] We can find that the k values decreased from $PBSEG_{10K-38}$ to $PBSEG_{10K-50}$, $PBSEG_{10K-58}$, $PBSEG_{6K-61}$, and $PBSEG_{2K-60}$ irrespective of the cooling rates, as shown in Table II, which was consistent with the decrease of T_c values or crystallizability.

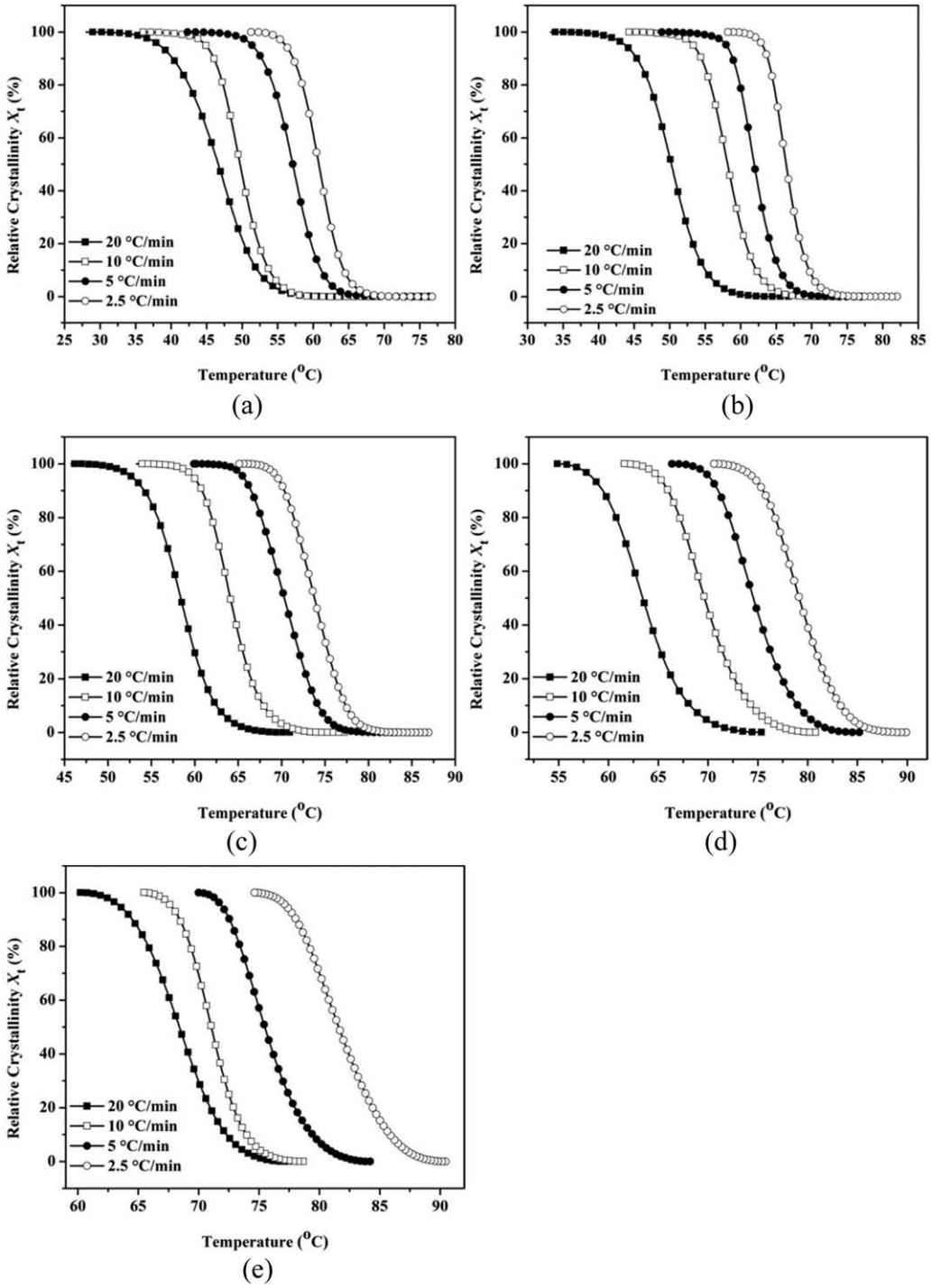

Figure 3. Relative crystallinity versus temperatures of PBS segment within (a) $PBSEG_{2K\text{-}60}$, (b) $PBSEG_{6K\text{-}61}$, (c) $PBSEG_{10K\text{-}58}$, (d) $PBSEG_{10K\text{-}50}$, and (e) $PBSEG_{10K\text{-}38}$ at different cooling rates.

During the nonisothermal crystallization process, the relation between t and T is given by[53]

$$t = \frac{T_0 - T}{\varphi} \tag{5}$$

To get further insight of the difference of crystallization kinetics between PBSEGs each other, X_t versus t and Avrami plots of five samples were put together as $\varphi = 10°C/min$ to analysis, illustrated in Figure 5. It can be seen that the typical sigmoidal shape curves were obtained. The longest crystallization time was needed for the sample $PBSEG_{2K\text{-}60}$, and the least for $PBSEG_{10K\text{-}38}$, suggesting that the PBS segment within $PBSEG_{2K\text{-}60}$ and $PBSEG_{10K\text{-}38}$ had the lowest and fastest crystallization rates, respectively. It took PBS segment within $PBSEG_{2K\text{-}60}$ around 3.4 min to complete crystallization; whereas, for the $PBSEG_{10K\text{-}38}$

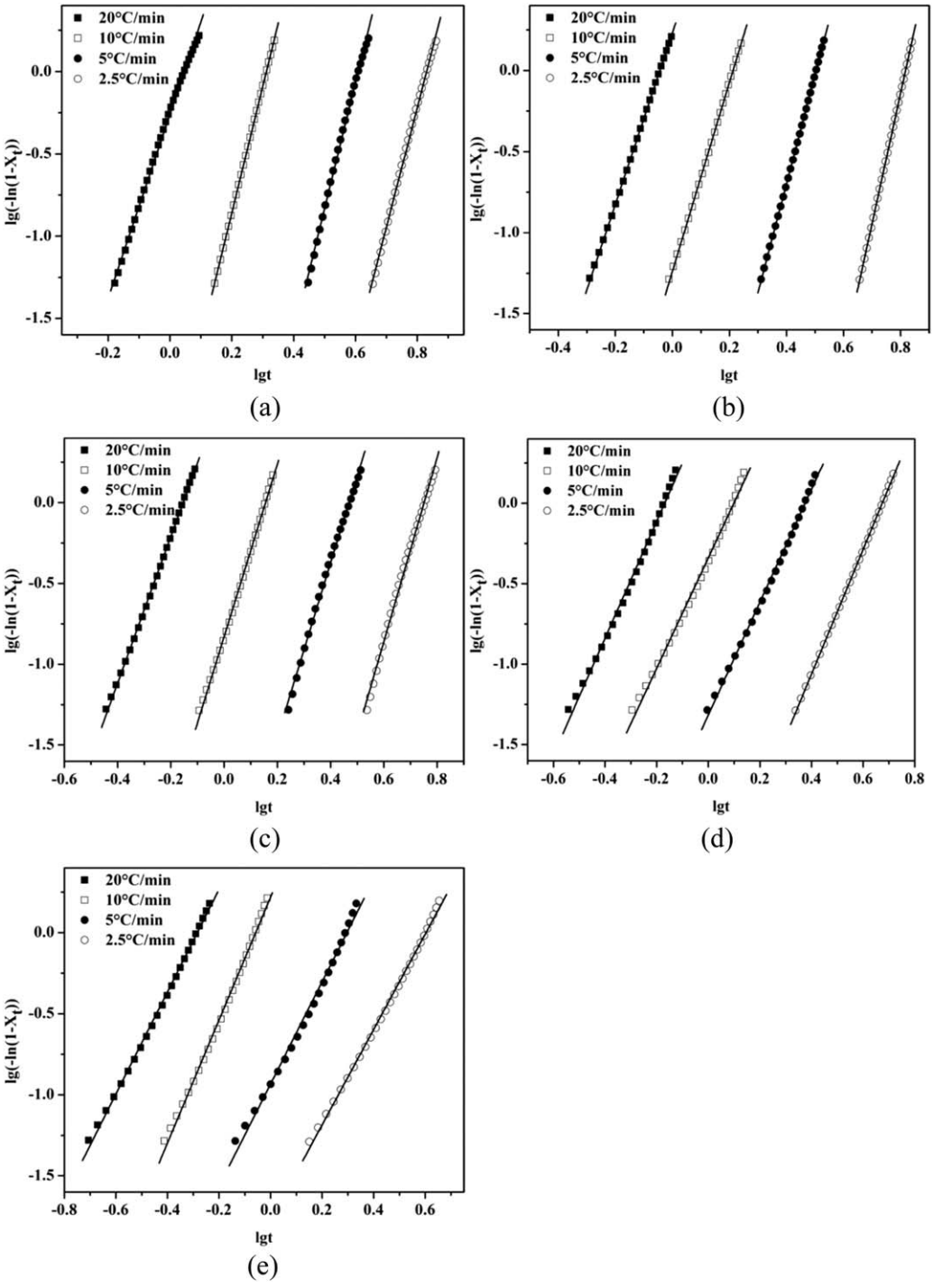

Figure 4. Avrami plots of PBS segment within (a) $PBSEG_{2K\text{-}60}$, (b) $PBSEG_{6K\text{-}61}$, (c) $PBSEG_{10K\text{-}58}$, (d) $PBSEG_{10K\text{-}50}$, and (e) $PBSEG_{10K\text{-}38}$ during nonisothermal crystallization.

sample, the time required to finish crystallization decreased to about 1.2 min at the same cooling rate. Additionally, about 2.9, 2.4, and 1.9 min were needed to finish crystallization for the PBS segment within $PBSEG_{6K\text{-}61}$, $PBSEG_{10K\text{-}58}$, and $PBSEG_{10K\text{-}50}$, respectively. The other cooling rates as $\varphi = 5°C/min$ showed similar behavior (Supporting Information Figure S1). From the results, it can be deduced that the crystallization rate reduced with the order of $PBSEG_{10K\text{-}38}$, $PBSEG_{10K\text{-}50}$, $PBSEG_{10K\text{-}58}$, $PBSEG_{6K\text{-}61}$, and $PBSEG_{2K\text{-}60}$, according to the above discussions.

Because of the various values of n, we cannot directly compare overall crystallization rate for different samples through the values of Z. Just like isothermal crystallization kinetics, the half-time of crystallization ($t_{1/2}$) defined as the time needed to achieve 50% of the complete crystallinity, which is inverse with

Table II. Nonisothermal Crystallization Parameter for PBS Segment of PBSEGs Obtained by the Avrami Method

Sample	Cooling rate (°C/min)	n	Z (min^{-n})	k (min^{-1})
$PBSEG_{2K\text{-}60}$	2.5	7.28	9.04×10^{-7}	0.14
	5	7.66	2.18×10^{-5}	0.25
	10	7.67	4.06×10^{-3}	0.49
	20	5.59	5.52×10^{-1}	0.90
$PBSEG_{6K\text{-}61}$	2.5	8.04	2.66×10^{-7}	0.15
	5	6.71	4.15×10^{-4}	0.31
	10	5.83	5.76×10^{-2}	0.61
	20	5.29	1.71	1.11
$PBSEG_{10K\text{-}58}$	2.5	5.68	5.37×10^{-5}	0.18
	5	5.37	3.00×10^{-3}	0.34
	10	5.33	1.48×10^{-1}	0.70
	20	4.54	5.01	1.43
$PBSEG_{10K\text{-}50}$	2.5	3.87	2.44×10^{-3}	0.21
	5	3.51	4.82×10^{-2}	0.42
	10	3.43	4.58×10^{-1}	0.80
	20	3.63	4.12	1.48
$PBSEG_{10K\text{-}38}$	2.5	2.94	1.68×10^{-2}	0.25
	5	3.15	1.17×10^{-1}	0.51
	10	3.79	1.66	1.14
	20	3.15	7.90	1.93

overall crystallization rate; or the reciprocal value of $t_{1/2}$ (i.e., $1/t_{1/2}$) is usually employed to represent the crystallization rate of polymer directly. The value of $t_{1/2}$ can be directly obtained from the relative crystallinity plots. Thus, here, $t_{1/2}$ and $1/t_{1/2}$ are introduced to describe the nonisothermal crystallization kinetics. The value of $t_{1/2}$ can be achieved by

$$t_{1/2}=\left(\frac{\ln 2}{Z}\right)^{1/n} \tag{6}$$

The values of $t_{1/2}$ and $1/t_{1/2}$ calculated by eq. (6) were summarized in Figure 6. $t_{1/2}$ of PBS segment within $PBSEG_{10K\text{-}38}$ was 3.54 min, which increased to 4.30, 5.29, 6.28, and 6.43 min at a cooling rate of 2.5°C/min for $PBSEG_{10K\text{-}50}$, $PBSEG_{10K\text{-}58}$, $PBSEG_{6K\text{-}61}$, and $PBSEG_{2K\text{-}60}$, respectively; and the value of $1/t_{1/2}$ decreased from 0.28 min^{-1} to 0.23, 0.19, 0.16, and 0.15 min^{-1} for $PBSEG_{10K\text{-}38}$, $PBSEG_{10K\text{-}50}$, $PBSEG_{10K\text{-}58}$, $PBSEG_{6K\text{-}61}$, and $PBSEG_{2K\text{-}60}$, respectively. The values of $t_{1/2}$ and $1/t_{1/2}$ also showed the same alteration trend under other cooling rates. The results indicated that the crystallization rate of PBS segment within PBSEG decreased with the content of PBS segment and/or L_{PBS}.

The Ozawa equation is derived from Avrami theory and can be used to describe the kinetics of nonisothermal crystallization process. In this approach, the nonisothermal crystallization process is the result of infinite number of small isothermal crystallization steps, on the assumption that, the nonisothermal process consists of innumerable isothermal crystallization processes. The Ozawa equation can be expressed as

$$\lg\left(-\ln\left(1-X_t\right)\right)=\lg K(T)-m\lg\varphi \tag{7}$$

where $K(T)$ is called the cooling or heating function of the process, which is related to the overall crystallization rate and indicates how fast crystallization occurs, and m is the Ozawa component that depends on the crystal growth and nucleation mechanism.[54] Figure 7 shows the plots of $\lg(-\ln(1-X_t))$ versus $\lg\varphi$ for PBS segment within $PBSEG_{6K\text{-}61}$ and $PBSEG_{10K\text{-}58}$. It can be seen that no straight lines could be obtained from $\lg(-\ln(1-X_t))$ as a function of $\lg\varphi$ at given temperatures. The results suggest that the Ozawa equation is not suitable to formulate the nonisothermal crystallization kinetics of the PBS segment within PBSEG, which is similar with other reports.[55–59]

In general, it is difficult to describe nonisothermal crystallization using a single equation, as there are a lot of parameters which have to be taken into account simultaneously. The Mo method, combining the Ozawa and Avrami equations, is almost a universal method and widely used to study nonisothermal crystallization kinetics of polymer.[58–62] It is expressed as

$$\lg\varphi=\lg F(T)-\alpha\lg t \tag{8}$$

where the parameter $F(T)$ is equal to $[K(T)/Z]^{1/m}$. Here, $K(T)$ is the Ozawa cooling function at temperature T, Z is Avrami crystallization rate constant, and α equals to n/m, where n and m are Avrami and Ozawa exponents, respectively. The physical meaning of $F(T)$ is that the value of cooling rate has to be chosen in a unit crystallization time when the measured system reaches a certain degree of crystallinity.[63] A high value of $F(T)$ corresponds to low crystallization rate. According to eq. (8), the plots of $\lg\varphi$ versus $\lg t$ gave a straight line at a given degree of crystallinity, as displayed in Figure 8. $F(T)$ and α were obtained from the intercept and slope, respectively. From Figure 8, we can conclude that there is a good linear relationship between $\lg\varphi$ and $\lg t$, as the adjusted R^2 values of almost all the straight lines were >0.99. The results indicated that Mo method can be successfully applied to describe the nonisothermal crystallization process of PBS segment within PBSEG. The values of $F(T)$ and α obtained from these straight lines were listed in Table III. It can be seen that $F(T)$ increased with the relative degree of crystallinity for all samples. In addition, the large value of $F(T)$ means that polymer crystallizes more slowly at a certain crystallinity. From the values of $F(T)$ in Table III, the order of crystallization rate was $PBSEG_{10K\text{-}38} < PBSEG_{10K\text{-}50} < PBSEG_{10K\text{-}58} < PBSEG_{6K\text{-}61} < PBSEG_{2K\text{-}60}$, which was consistent with that of $t_{1/2}$. The values of α were almost constant for a given sample. The average α of PBS segment within $PBSEG_{10K\text{-}38}$, $PBSEG_{10K\text{-}50}$, $PBSEG_{10K\text{-}58}$, $PBSEG_{6K\text{-}61}$, and $PBSEG_{2K\text{-}60}$ were 1.14, 1.03, 0.99, 1.07, and 0.99, respectively. The average values of α having a narrow range (from 0.99 to 1.14) suggested that the crystallization behavior of PBS segment within PBSEG was almost not changed.

Nonisothermal Crystallization Kinetics Study of PEG Segment Within PBSEG

The methods of studying nonisothermal crystallization kinetics of PEG segment within PBSEG bear an analogy to PBS segment. Nonisothermal crystallization curves of PEG segment within $PBSEG_{6K\text{-}61}$ and $PBSEG_{10K\text{-}58}$ (as two studied examples), as

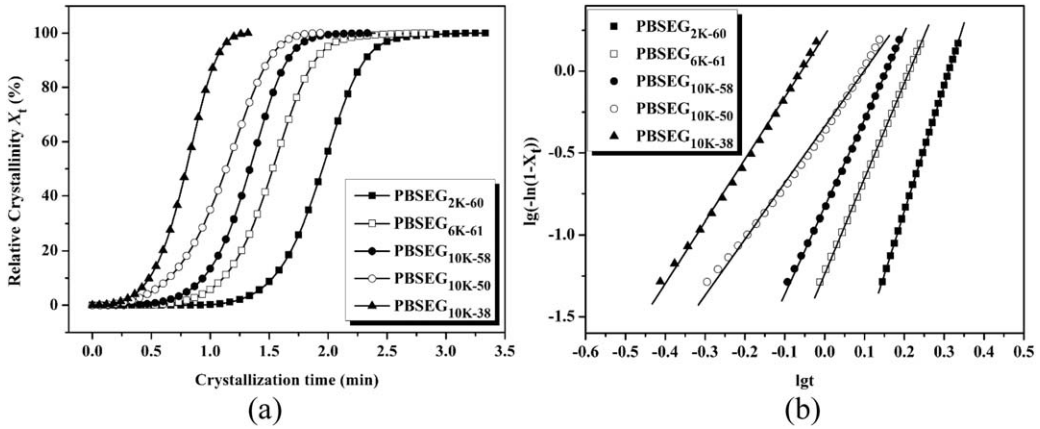

Figure 5. (a) Plots of relative crystallinity versus crystallization time and (b) Avrami plots of PBS segment within PBSEG during nonisothermal crystallization at 10°C/min.

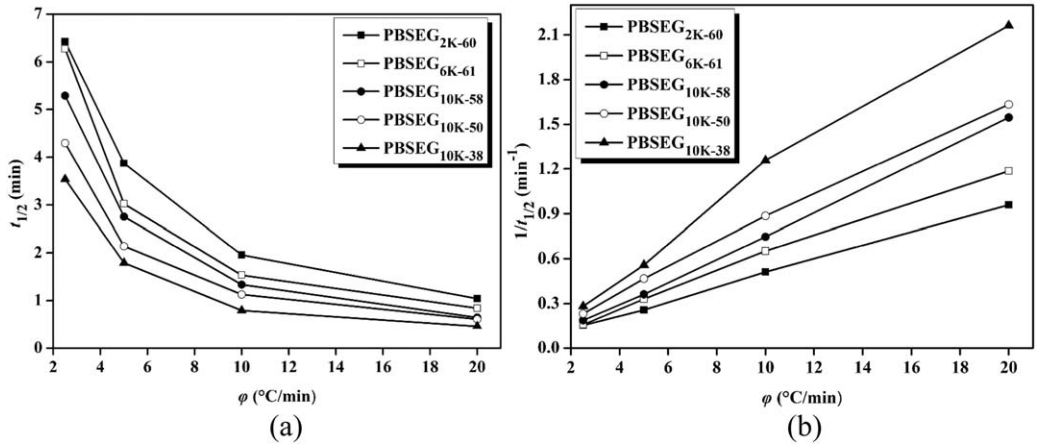

Figure 6. The values of (a) $t_{1/2}$ and (b) $1/t_{1/2}$ of PBS segment within PBSEG at various cooling rates.

typical examples, moved to lower temperature range compared with PBS segment (Supporting Information Figure S2). As the cooling rate increasing, the crystallization curves became broader and shifted to lower temperature. T_c of the five samples at various cooling rates was summarized in Figure 9. The order of PEG segment T_c within PBSEG was $PBSEG_{10K\text{-}38}<PBSEG_{10K\text{-}50}<PBSEG_{10K\text{-}58}$, and $PBSEG_{2K\text{-}60}<PBSEG_{6K\text{-}61}<PBSEG_{10K\text{-}58}$ at a given cooling rate for the two series, respectively. On the one hand, T_c of PEG segment decreased from $PBSEG_{10K\text{-}58}$ to $PBSEG_{10K\text{-}50}$ and $PBSEG_{10K\text{-}38}$ because of the decrease of F_{PEG}.

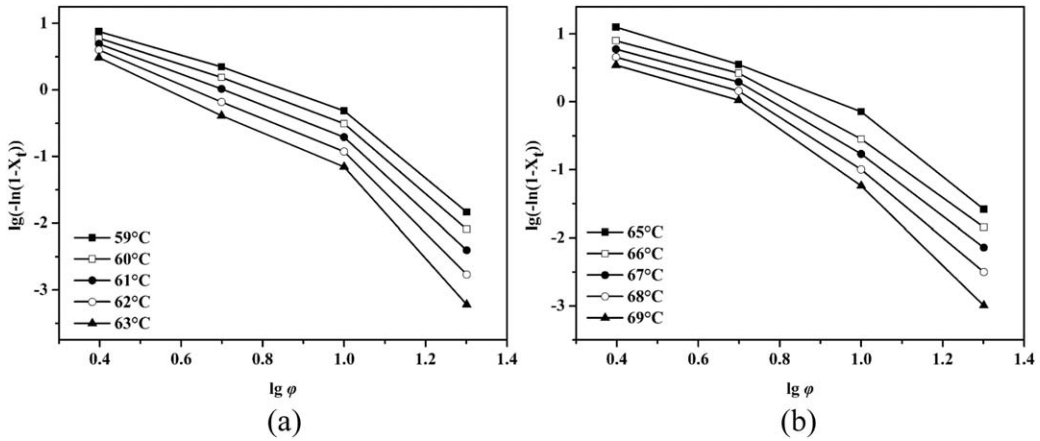

Figure 7. Plots of $\lg(-\ln(1-X_t))$ versus $\log \phi$ at the indicated temperatures of PBS segment within (a) $PBSEG_{6K\text{-}61}$ and (b) $PBSEG_{10K\text{-}58}$.

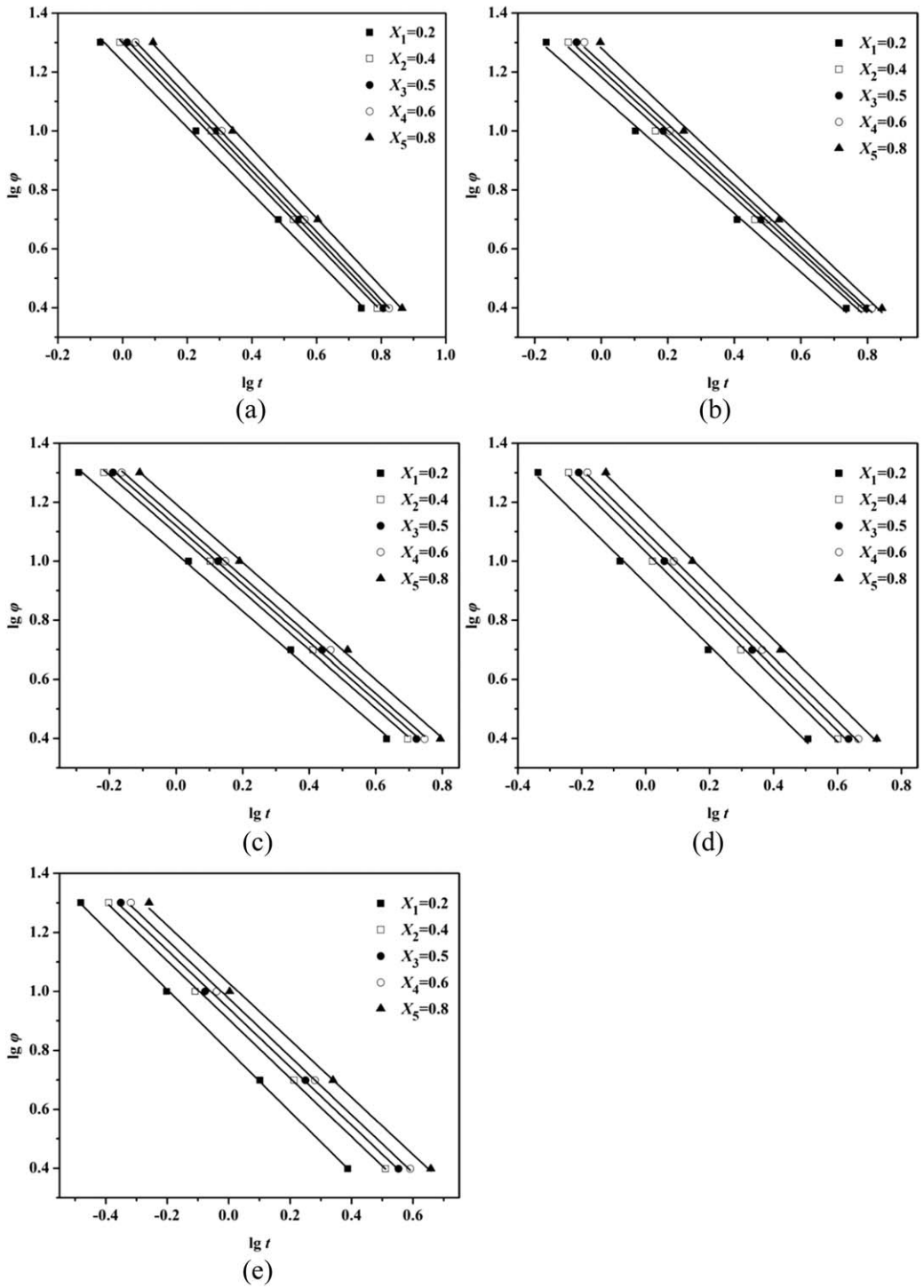

Figure 8. Plots of lg ϕ versus lg t of PBS segment within (a) $PBSEG_{2K\text{-}60}$, (b) $PBSEG_{6K\text{-}61}$, (c) $PBSEG_{10K\text{-}58}$, (d) $PBSEG_{10K\text{-}50}$, and (e) $PBSEG_{10K\text{-}38}$ during nonisothermal crystallization.

On the other hand, shorter PEG chain segment length resulted in the decrease of T_c of PEG segment from $PBSEG_{10K\text{-}58}$ to $PBSEG_{6K\text{-}61}$ and $PBSEG_{2K\text{-}60}$. The results are accorded with previous work.[19]

Similar to the treatment of PBS segment within PBSEG, the Avrami equation was also used to analyze PEG segment. Sigmoidal shape curves (Supporting Information Figure S3) were obtained from X_t versus temperature and plots of $\lg(-\ln(1-X_t))$ versus lg t (Supporting Information Figure S4) gave a series of parallel lines. The results suggested that Avrami method could also be used to understand the nonisothermal crystallization kinetics of PEG segment. The values of Z, n, and k were derived from these parallel lines (Supporting

Table III. Nonisothermal Crystallization Kinetics Parameters for PBS Segment of PBSEGs at Different Degrees of Crystallinity by the Mo Method

	$PBSEG_{2K-60}$		$PBSEG_{6K-61}$		$PBSEG_{10K-58}$		$PBSEG_{10K-50}$		$PBSEG_{10K-38}$	
X_t	$F(T)$	α	$F(T)$	α	$F(T)$	α	$F(T)$	A	$F(T)$	α
0.2	17.38	1.12	13.18	1.00	10.72	0.98	8.52	1.07	6.31	1.03
0.4	19.95	1.14	15.14	1.02	12.30	0.99	10.72	1.07	8.13	1.00
0.5	20.89	1.14	16.22	1.03	13.18	0.99	11.75	1.07	8.71	0.99
0.6	22.39	1.15	16.98	1.04	13.80	0.99	12.59	1.07	9.55	0.99
0.8	25.70	1.17	19.05	1.06	15.49	0.99	14.45	1.07	10.71	0.98

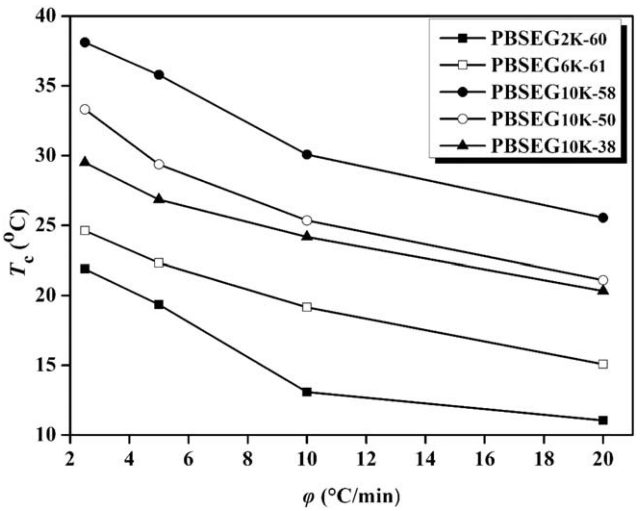

Figure 9. The crystallization peak temperature of PEG segment within PBSEGs at various cooling rates.

Information Table S1). Z increased with cooling rate for all the samples. The average values of n were 4.04, 3.59, 3.22, 3.33, and 3.44 for PEG segment within $PBSEG_{2K-60}$, $PBSEG_{6K-61}$, $PBSEG_{10K-58}$, $PBSEG_{10K-50}$, and $PBSEG_{10K-38}$, respectively. The narrow range of n value indicated the crystallization mechanism of PEG segment within all samples was similar. For these five samples, the crystallization behavior shows similar after the PBS segment crystallizing. The fact that the morphology of PEG segment showed 2-dimentional growth on previous PBS crystals also proves the similar crystallization behavior. The order of values k was $PBSEG_{10K-38}<PBSEG_{10K-50}<PBSEG_{10K-58}$, and $PBSEG_{2K-60}<PBSEG_{6K-61}<PBSEG_{10K-58}$ for the two series, respectively. It was consistent with the order of T_c values. Under the same cooling rate, more time was needed to complete crystallization for PBSEG with small value of $M_{n,PEG}$ or F_{PEG} (Supporting Information Figure S5).

As we cannot compare the crystallization rate with Z because of the different n, $t_{1/2}$, and $1/t_{1/2}$ obtained from the values of Z and n, which were summarized in Figure 10. $t_{1/2}$ of PEG segment within $PBSEG_{10K-58}$ was 1.68 min, which increased to 2.00 and 2.83 min at cooling rate of 2.5°C/min for $PBSEG_{6K-61}$ and $PBSEG_{2K-60}$, respectively; and it decreased to 2.47 and 4.38 min for $PBSEG_{10K-50}$ and $PBSEG_{10K-38}$ at the same cooling rate, respectively. Besides, $1/t_{1/2}$ of PEG segment within $PBSEG_{10K-58}$ to $PBSEG_{6K-61}$, $PBSEG_{2K-60}$, $PBSEG_{10K-50}$, and $PBSEG_{10K-38}$ decreased from 0.60 min^{-1} to 0.50, 0.35, 0.40, and 0.23 min^{-1} from, respectively. The values of $t_{1/2}$ and $1/t_{1/2}$ also showed the same alteration trend under other cooling rates. The results indicate that the crystallization rate of PEG segment within PBSEGs decreased with $M_{n,PEG}$ or F_{PEG}.

We have also tried to use Ozawa method to describe the nonisothermal crystallization kinetics of PEG segment within PBSEG. Yet no straight lines could be obtained when plotting $\lg(-\ln(1-X_t))$ versus $\lg \phi$, suggesting that the Ozawa equation is also unable to study nonisothermal crystallization kinetics of PEG segment within PBSEG. Mo method was applied to describe the nonisothermal crystallization process of PEG

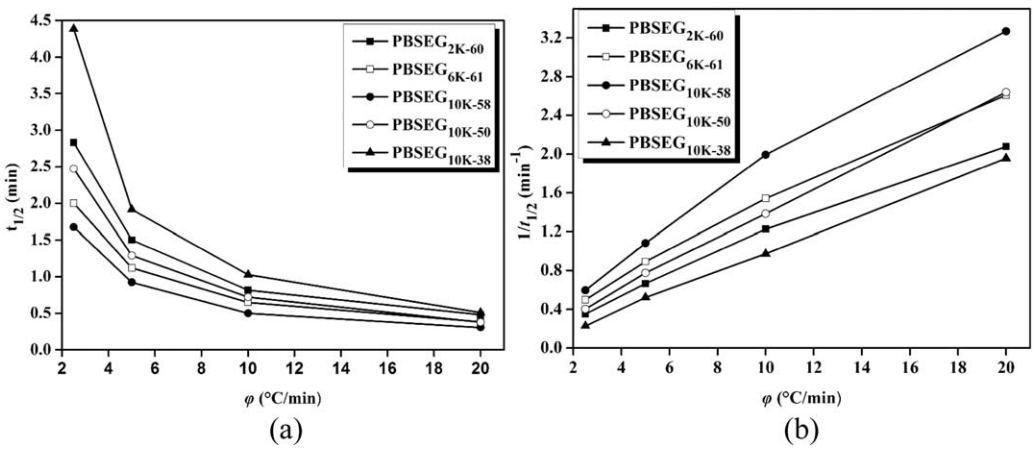

Figure 10. The values of (a) $t_{1/2}$ and (b) $1/t_{1/2}$ of PEG segment within PBSEG at various cooling rates.

segment within PBSEG (Supporting Information Figure S6). Obviously, there was a good linear relationship between lg ϕ and lg t because of the high adjusted R^2 values of straight lines, indicating that the Mo method could be successfully applied to describe the nonisothermal crystallization process of PEG segment within PBSEG. The slope and intercept of the plots yielded α and lg $F(T)$, respectively (Supporting Information Table S2). $F(T)$ increased with the relative degree of crystallinity for all samples. According to Supporting Information Table S2, the order of crystallization rate was $PBSEG_{10K-38}<PBSEG_{10K-50}<PBSEG_{10K-58}$, and $PBSEG_{2K-60}<PBSEG_{6K-61}<PBSEG_{10K-58}$ for the two series, respectively, according with result of $t_{1/2}$. The values of α were almost constant for a given sample.

CONCLUSIONS

In conclusion, nonisothermal crystallization kinetics of both PBS and PEG segments within PBSEG were investigated by DSC, and were studied by Avrami, Ozawa, and Mo methods. The results showed that Avrami can successfully analyze the nonisothermal crystallization kinetics of both PBS and PEG segments within PBSEG. The values Avrami exponent n of PBS segment were higher than that of PEG segment, especially for samples $PBSEG_{2K-60}$ and $PBSEG_{6K-61}$. The crystallization rate of PBS segment within PBSEG decreased with content of PBS segment and/or L_{PBS}, while the decrease of $M_{n,PEG}$ or F_{PEG} would result in small the crystallization rate value of PEG segment. Besides, the Ozawa method could not be used to describe both PBS and PEG segments within PBSEG. Furthermore, the Mo method was a good method to analyze the nonisothermal crystallization kinetics of both PBS and PEG segments, and the alternate trend of the crystallization rate in the five samples were consistent with Avrami method. Based on these data, we can get some basic guidance to process the double crystalline blocks copolymers.

ACKNOWLEDGMENTS

This work was supported financially by the National Science Foundation of China (51273120, 51121001), and Program for Changjiang Scholars and Innovative Research Team in University of Ministry of Education o f China (IRT1026).

REFERENCES

1. Chandra, R.; Rustgi, R. *Prog. Polym. Sci.* **1998**, *23*, 1273.
2. Masahiko, O. *Prog. Polym. Sci.* **2002**, *27*, 87.
3. Sinha Ray, S.; Bousmina, M. *Prog. Polym. Sci.* **2005**, *50*, 962.
4. Nair, L. S.; Laurencin, C. T. *Prog. Polym. Sci.* **2007**, *32*, 762.
5. Lim, L. T.; Auras, R.; Rubino, M. *Prog. Polym. Sci.* **2008**, *33*, 820.
6. Gross, R. A.; Kalra, B. *Science* **2002**, *297*, 803.
7. Langer, R.; Tirrell, D. A. *Nature* **2004**, *428*, 487.
8. Takashi, F. *Polym. Degrad. Stab.* **1998**, *59*, 209.
9. Papageorgiou, G. Z.; Bikiaris, D. N. *Biomacromolecules* **2007**, *8*, 2437.
10. Papageorgiou, G. Z.; Bikiaris, D. N. *Polymer* **2005**, *46*, 12081.
11. Xu, J.; Guo, B. H. Microbial Succinic Acid, Its Polymer Poly(butylene succinate), and Applications. In: Plastics from Bacteria, Chen, G. G. -Q., Ed. Springer: Berlin / Heidelberg, **2010**; Vol. *14*, p 347.
12. Chan, N.; Khorsand, B.; Aleksanian, S.; Oh, J. K. *Chem. Commun.* **2013**, *49*, 7534.
13. Wei, X.; Gong, C.; Gou, M.; Fu, S.; Guo, Q.; Shi, S.; Luo, F.; Guo, G.; Qiu, L.; Qian, Z. *Int. J. Pharm.* **2009**, *381*, 1.
14. Jeong, B.; Lee, D. S.; Shon, J. I.; Bae, Y. H.; Kim, S. W. *J. Polym. Sci., Part A: Polym. Chem.* **1999**, *37*, 751.
15. Jeong, B.; Bae, Y. H.; Lee, D. S.; Kim, S. W. *Nature* **1997**, *388*, 860.
16. Zhou, S.; Deng, X.; Yang, H. *Biomaterials* **2003**, *24*, 3563.
17. Pepic, D.; Zagar, E.; Zigon, M.; Krzan, A.; Kunaver, M.; Djonlagic, J. *Eur. Polym. J.* **2008**, *44*, 904.
18. Lu, X.; Zeng, J.-B.; Huang, C.-L.; Wang, Y.-Z. *Ind. Eng. Chem. Res.* **2012**, *51*, 8262.
19. Huang, C. L.; Jiao, L.; Zhang, J. J.; Zeng, J. B.; Yang, K. K.; Wang, Y. Z. *Polym. Chem.* **2012**, *3*, 800.
20. Huang, C. L.; Jiao, L.; Zeng, J. B.; Zhang, M.; Xiao, L. P.; Yang, K. K.; Wang, Y. Z. *Polymer* **2012**, *53*, 3780.
21. Huang, C. L.; Jiao, L.; Zeng, J. B.; Zhang, J. J.; Yang, K. K.; Wang, Y. Z. *J. Phys. Chem. B* **2013**, *117*, 10665.
22. Cho, K.; Lee, J.; Kwon, K. *J. Appl. Polym. Sci.* **2001**, *79*, 1025.
23. Zeng, J. B.; Liu, C.; Liu, F. Y.; Li, Y. D.; Wang, Y. Z. *Ind. Eng. Chem. Res.* **2010**, *49*, 9870.
24. Achilias, D. S.; Papageorgiou, G. Z.; Karayannidis, G. P. *J. Polym. Sci., Part B: Polym. Phys.* **2004**, *42*, 3775.
25. Papageorgiou, G. Z.; Achilias, D. S.; Bikiaris, D. N. *Macromol. Chem. Phys.* **2007**, *208*, 1250.
26. Vassiliou, A. A.; Papageorgiou, G. Z.; Achilias, D. S.; Bikiaris, D. N. *Macromol. Chem. Phys.* **2007**, *208*, 364.
27. Li, J.; Zhou, C.; Wang, G.; Tao, Y.; Liu, Q.; Li, Y. *Polym. Test.* **2002**, *21*, 583.
28. Li, J.; Zhou, C.; Gang, W. *Polym. Test.* **2003**, *22*, 217.
29. Qiu, Z.; Ikehara, T.; Nishi, T. *Polymer* **2003**, *44*, 5429.
30. Qiu, Z.; Fujinami, S.; Komura, M.; Nakajima, K.; Ikehara, T.; Nishi, T. *Polym. J.* **2004**, *36*, 642.
31. Supaphol, P. *J. Appl. Polym. Sci.* **2000**, *78*, 338.
32. Supaphol, P.; Spruiell, J. E. *J. Appl. Polym. Sci.* **2000**, *75*, 337.
33. Apiwanthanakorn, N.; Supaphol, P.; Nithitanakul, M. *Polym. Test.* **2004**, *23*, 817.
34. Supaphol, P.; Apiwanthanakorn, N. *J. Polym. Sci., Part B: Polym. Phys.* **2004**, *42*, 4151.
35. Nofar, M.; Zhu, W.; Park, C. B.; Randall, J. *Ind. Eng. Chem. Res.* **2011**, *50*, 13789.
36. Bogdanov, B.; Vidts, A.; Schacht, E.; Berghmans, H. *Macromolecules* **1999**, *32*, 726.
37. Albuerne, J.; Márquez, L.; Müller, A. J.; Raquez, J. M.; Degée, P.; Dubois, P.; Castelletto, V.; Hamley, I. W. *Macromolecules* **2003**, *36*, 1633.

38. Müller, A. J.; Albuerne, J.; Esteves, L. M.; Marquez, L.; Raquez, J.-M.; Degée, P.; Dubois, P.; Collins, S.; Hamley, I. W. *Macromol. Symp.* **2004**, *215*, 369.
39. Dyke, C. A.; Tour, J. M. *J. Phys. Chem. A* **2004**, *108*, 11151.
40. He, C.; Sun, J.; Ma, J.; Chen, X.; Jing, X. *Biomacromolecules* **2006**, *7*, 3482.
41. He, C.; Sun, J.; Zhao, T.; Hong, Z.; Zhuang, X.; Chen, X.; Jing, X. *Biomacromolecules* **2006**, *7*, 252.
42. Van Horn, R. M.; Zheng, J. X.; Sun, H.-J.; Hsiao, M.-S.; Zhang, W.-B.; Dong, X.-H.; Xu, J.; Thomas, E. L.; Lotz, B.; Cheng, S. Z. D. *Macromolecules* **2010**, *43*, 6113.
43. Hamley, I. W.; Castelletto, V.; Castillo, R. V.; ller, A. J. M.; Martin, C. M.; Pollet, E.; Dubois, P. *Macromolecules* **2005**, *38*, 463.
44. Castillo, R. V. n.; Muüller, A. J.; Raquez, J.-M.; Dubois, P. *Macromolecules* **2010**, *43*, 4149.
45. Castillo, R. V.; Müller, A. J. *Prog. Polym. Sci.* **2009**, *34*, 516.
46. Papageorgiou, G. Z.; Grigoriadou, I.; Andriotis, E.; Bikiaris, D. N.; Panayiotou, C. *Ind. Eng. Chem. Res.* **2013**, *52*, 11948.
47. Zeng, J. B.; Srinivansan, M.; Li, S. L.; Narayan, R.; Wang, Y. Z. *Ind. Eng. Chem. Res.* **2011**, *50*, 4471.
48. Herrero, C. R.; Acosta, J. L. *Polym. J.* **1994**, *26*, 786.
49. Cebe, P. *Polym. Compos.* **1988**, *9*, 271.
50. de Juana, R.; Jauregui, A.; Calahorra, E.; Cortázar, M. *Polymer* **1996**, *37*, 3339.
51. Avrami, M. *J. Chem. Phys.* **1939**, *7*, 1103.
52. Martínez-Palau, M.; Franco, L.; Puiggalí, J. *J. Polym. Sci., Part B: Polym. Phys.* **2008**, *46*, 121.
53. Avrami, M. *J. Chem. Phys.* **1940**, *8*, 212.
54. Ozawa, T. *Polymer* **1971**, *12*, 150.
55. Gan, Z.; Zhang, J.; Jiang, B. *J. Appl. Polym. Sci.* **1997**, *63*, 1793.
56. Bhattarai, N.; Kim, H. Y.; Cha, D. I.; Lee, D. R.; Yoo, D. I. *Eur. Polym. J.* **2003**, *39*, 1365.
57. Xu, W.; Ge, M.; He, P. *J. Appl. Polym. Sci.* **2001**, *82*, 2281.
58. Wang, D. Y.; Wei, L. L.; Ge, X. G.; Yang, K. K.; Wang, X. L.; Wang, Y. Z. *J. Macromol. Sci. Phys.* **2009**, *48*, 927.
59. Zheng, G. C.; Ding, S. D.; Zeng, J. B.; Wang, Y. Z.; Li, Y. D. *J. Macromol. Sci. B* **2010**, *49*, 269.
60. Wang, Y.; Shen, C.; Li, H.; Li, Q.; Chen, J. *J. Appl. Polym. Sci.* **2004**, *91*, 308.
61. Wan, T.; Chen, L.; Chua, Y. C.; Lu, X. *J. Appl. Polym. Sci.* **2004**, *94*, 1381.
62. Xu, W.; Ge, M.; He, P. *J. Polym. Sci., Part B: Polym. Phys.* **2002**, *40*, 408.
63. Liu, T.; Mo, Z.; Wang, S.; Zhang, H. *Polym. Eng. Sci.* **1997**, *37*, 568.